Journal of Macromolecular Science, Part A
Publication details, including instructions for authors and subscription information:
http://www.informaworld.com/smpp/title~content=t713597274

Structural Studies on Polymers as Prerequisites for Degradation

Josef Schurz[a]; Peter Zipper[a]; Jürgen Lenz[b]
[a] Institute of Physical Chemistry, University of Graz, Graz, Austria [b] Chemie Lenzing AG Lenzing, Austria

To cite this Article Schurz, Josef , Zipper, Peter and Lenz, Jürgen(1993) 'Structural Studies on Polymers as Prerequisites for Degradation', Journal of Macromolecular Science, Part A, 30: 9, 603 — 619
To link to this Article: DOI: 10.1080/10601329308021249
URL: http://dx.doi.org/10.1080/10601329308021249

J.M.S.—PURE APPL. CHEM., A30(9 & 10), pp. 603–619 (1993)

STRUCTURAL STUDIES ON POLYMERS AS PREREQUISITES FOR DEGRADATION

JOSEF SCHURZ and PETER ZIPPER

Institute of Physical Chemistry
University of Graz
Graz, Austria

JÜRGEN LENZ

Chemie Lenzing AG
Lenzing, Austria

ABSTRACT

A review is given on some progress made in structural investigation of both synthetic and natural polymers with a view to their degradation. Some new results are presented which stress the importance of the so-called amorphous portion of polymers and its orientation for processing, properties, and degradation.

The structure of polymers determines their accessibility for degrading agents of both chemical and microbial origin. Structure determinations by means of x-rays are therefore an important prerequisite for degradation processes. For thermoplastic products, it is shown that both crystallinity and orientation vary significantly over both the cross section and the distance from the gate. Such changes are reported for polypropylene with a resolution of about 0.02 mm, and their origin is discussed. For regenerated cellulose fibers, structural differences exist between fibers spun according to whether the old viscose process or the new Lyocell process, which is favored on environmental grounds, is used. The kinetics of enzymatic degradation is significantly different for native and regenerated cellulose. An explanation for this finding is proposed.

INJECTION-MOLDED POLYPROPYLENE SAMPLES

The aim of these studies was to investigate the fine texture of injection-molded samples of polypropylene (PP), namely, their crystallinity and orientation, with the highest possible spatial resolution over the sample thickness and in dependence on the distance from the gate. To this end, test pieces (circular disks and rectangular plates of 2 mm thickness) were prepared in an injection molding machine from isotactic PP (Daplen KS10 and PT55 from PCD, Linz). Samples were cut from these pieces in the way shown in Fig. 1. Their dimensions ranged from 2.5 × 2.5 × 2 mm to 10 × 3 × 2 mm. They were irradiated with an x-ray beam of line-shaped cross-section of 2.5 mm × 60 μm in a Kratky camera. The irradiation was always parallel to the surface of the pieces, but either perpendicular or parallel or antiparallel to the flow direction. The wide-angle scattering of the samples was registered by means of a linear position sensitive detector (PSD) with an aperture of about 10°. The samples were scanned over their thickness in 20 μm steps, and for each step a scattering curve was taken. The setup is schematically shown in Fig. 1. Detailed descriptions of the procedure are given elsewhere [1, 2].

Though the experimental setup and the measurements themselves are quite simple, a wealth of information about different aspects of structure and texture in the moldings can be obtained from the measurements either directly or by applying sophisticated evaluation procedures. The most direct information concerns the het-

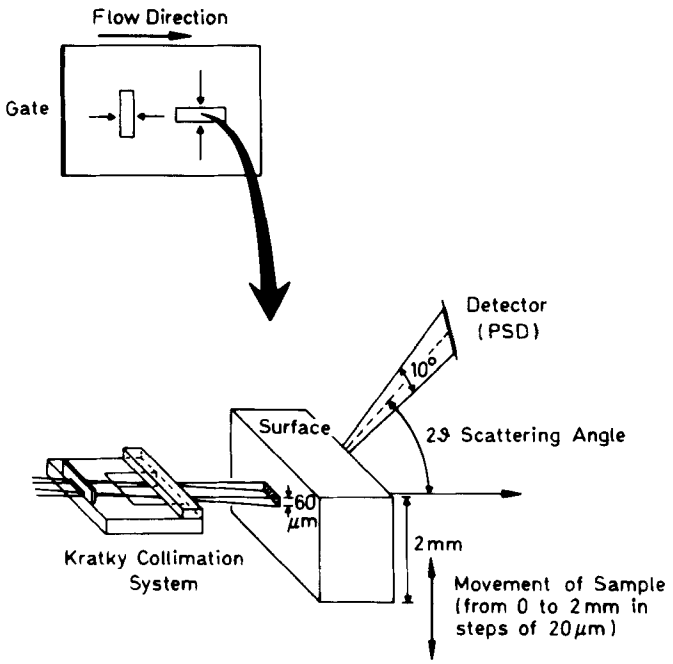

FIG. 1. Schematic diagrams showing the preparation of samples from test pieces and the experimental setup for the position-resolved wide-angle x-ray measurements.

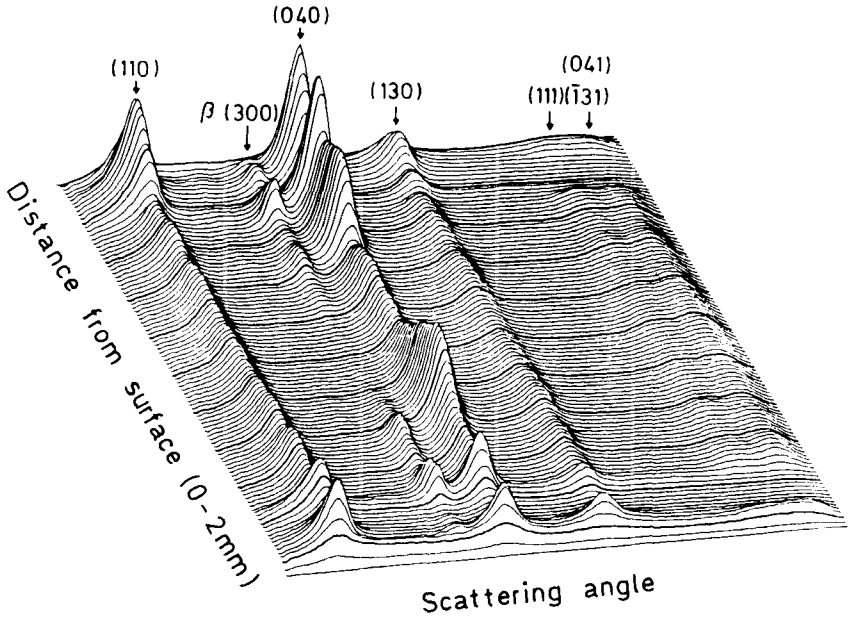

FIG. 2. Scattering relief: Wide-angle x-ray scattering curves (intensity as a function of scattering angle) plotted vs the distance from the surface. The sample was cut from an injection-molded Daplen KS10 disk (diameter 280 mm, thickness ≈ 2 mm), 40 mm from the gate. The x-ray beam was antiparallel to the direction of flow, and the sample was moved through the beam in steps of 20 μm from surface to surface.

erogeneity over the thickness of the samples, manifested by a number of different layers running parallel to the surface of the moldings. The multilayered structure of the cross section is a common feature of all moldings investigated in the course of our studies, while the details of this structure were found to vary considerably in dependence on the polymer grade, the processing conditions, and the position in the moldings (expressed by the distance from the gate). We observed, for instance, differences in the distribution of crystallite types (α-, β- and γ-PP; cf. Ref. 3), in the size of crystallites, in their orientation, and in the orientation of the noncrystalline portion. A few examples have been selected to illustrate the power and efficiency of our approach.

The output of the x-ray measurement on a sample is presented best in an intensity map, also called "scattering relief." Either we plot the data as scattering curves (that is, intensity as a function of scattering angle) with the depth d (distance from surface) as a parameter (Fig. 2 shows an example) or we present scattering profiles (that is, intensity as a function of depth) with the scattering angle as a parameter (Fig. 3). Intensity maps may be interpreted directly to yield qualitative or semiquantitive information about the texture of the sample.

Let us discuss Fig. 2 first. The scattering curves clearly show the reflections (110), (040), (130), and less pronounced (111), (T31), (041) of the predominant α-modification of PP, and (300) of β-PP. The intensity of the reflections varies over the thickness. A high intensity indicates a high degree of orientation and

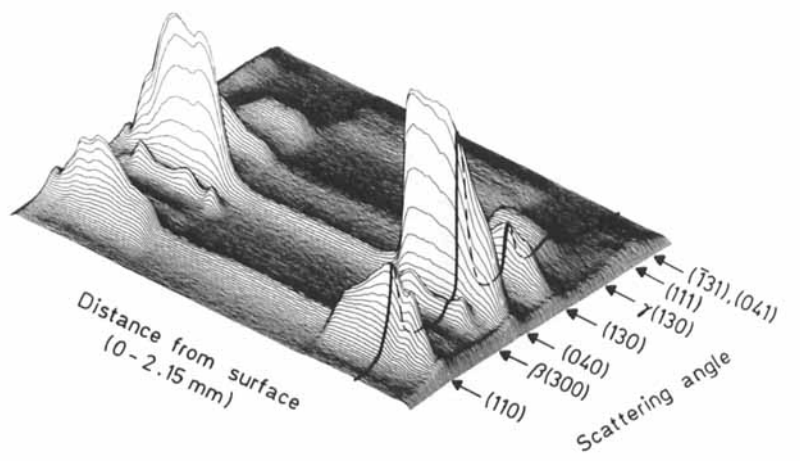

FIG. 3. Scattering relief: Wide-angle x-ray scattering profiles (intensity as a function of the distance from the surface) plotted vs the scattering angle. One additional scattering curve is drawn. The sample was cut from an injection-molded Daplen KS10 plate (230 × 70 × 2 mm), 100 mm from the gate. The x-ray beam was perpendicular to the flow direction.

good crystallization. We note that in general the intensity, and thus the degree of orientation, is higher near the surface and lower in the center of the cross section. We also note that the intensity distribution is not symmetrical around the center. As will be discussed later, the symmetry of the intensity distribution can depend on the direction of the x-ray beam (in the case of Fig. 2, the beam was antiparallel to the flow direction).

An example of scattering profiles is shown in Fig. 3. For one case, the scattering curve is also indicated. Here we see an intensity distribution which is nearly symmetrical around the center of the cross section. Figure 3 is derived from measurements with the x-ray beam perpendicular to the flow direction. For this direction the scattering profiles directly mirror the symmetry of the texture: high orientation near the surface, low orientation in the core. Again, the lattice planes are indicated. We note the occurrence of an additional reflection due to the γ-modification of PP. In this picture we also see a "skin layer" directly at the surface of the sample. Obviously, the crystallinity of this layer is rather low.

By means of considerations which are beyond the scope of this article, we can also derive quantitative information from the intensity maps if we compare either the intensities of different reflections [2] or the intensities of the same reflection measured with different directions of the x-ray beam [1]. In this way we obtain a variety of parameters which characterize, for instance, the state of orientation of crystallites, the relative amounts of various crystallite modifications, the size of crystallites, and the distances between lattice planes. We dispense with a presentation of all our data, and show only a few of them in Fig. 4.

Before we can discuss the features of Fig. 4 in detail, we must know that the PP samples investigated exhibit a fiber texture, with the fiber axis running roughly parallel to the direction of flow, though often with a certain inclination to it [1, 4, 5]. This inclination of the fiber axis causes a dissymmetry of the scattering relief

when the direction of the x-ray beam is parallel or antiparallel to the flow direction (cf. Fig. 2). We must further know that the α-PP crystallites, which represent folding crystallites, may assume different orientations relative to the fiber axis (the flow direction): they can be found in *c*-orientation (that is, the molecular chains are parallel to the flow direction) or in *a**-orientation, with the reciprocal lattice vector *a** in the flow direction [4, 6]. In both cases the *b*-direction of crystallites is perpendicular to the fiber axis.

In Fig. 4 we note a parameter A_{110} which is an indicator of the orientation of (110) lattice planes of α-PP crystallites ($A_{110} = 1$ if the planes of *c*-oriented crystallites are parallel to the flow direction [2]; cf. also Ref. 7); the parameter T_{040} is a measure of the degree of orientation of (040) lattice planes of *c*- or *a**-oriented α-crystallites parallel to the fiber axis; the parameter *C* quantifies the relative amount of *a**-orientation ($C = 1$ if α-crystallites assume pure *a**-orientation). Additionally are shown the parameter *B*, which is a measure of the content of β-PP ($B \approx 1$ for pure β-PP; cf. Ref. 8), and the parameter *G* that measures the content of γ-PP in a similar way. It is obvious that these parameters altogether provide a fairly good picture of the texture in the cross section of the sample.

Not only do the parameters shown in Fig. 4 exhibit considerable variations in dependence on the distance from the surface. The same also holds for the (apparent) crystallite dimensions determined from the half-widths of reflections, and we also have indications that certain variations of the lattice plane distances take place which would doubtlessly indicate slight lattice distortions. An additional variation of parameters is observed in dependence on the distance from the gate.

We found that the size of α-crystallites was about 15 to 25 nm along their

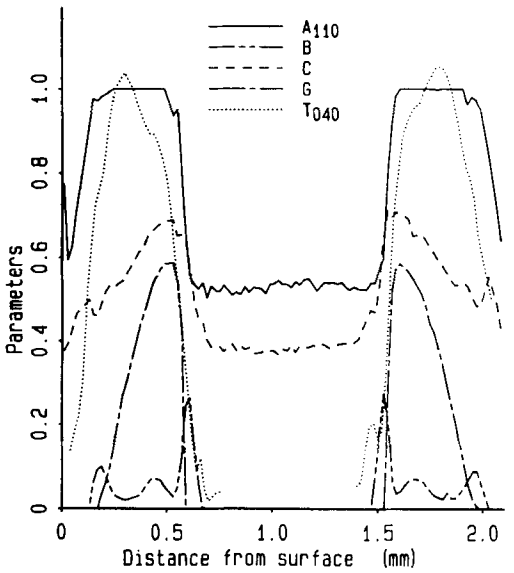

FIG. 4. Various parameters characterizing the texture in the Daplen KS10 sample from Fig. 2, plotted vs the distance from the surface. The meaning of the parameters is explained in the text.

b-direction, and similar but slightly lower crystallite dimensions were obtained along the normals to (110) and (130) lattice planes. We often found that the crystallites in the oriented zone near the surface (in the "boundary layer") were larger than those in the core. The crystallite size in the core was found to be rather independent of the distance from the gate, whereas in the boundary layer the size decreased with increasing distance. Also, a variation of crystallite size with the processing parameters (for instance, an increase with increasing injection pressure) was observed. The crystallite size along the *c*-direction cannot be determined directly from wide-angle reflections but has to be estimated from the long period reflections observed in small-angle patterns of the samples. We found long periods of about 15 nm. Thus, the α-crystallites are probably not very anisometric. In general, the crystal size of β-PP was found to exceed that of α-PP.

Our approach to texture analysis based on wide-angle scattering reliefs opened a way to study the background scattering also. This background is supposed to be caused by the noncrystalline, "amorphous" portion of the polymer, which is often regarded as rather uniform and hardly oriented. We found that this assumption is not true, and that this portion plays an important role for the mechanical properties of plastic pieces. In the course of evaluation of the scattering reliefs, we had to separate the "crystalline scattering" from the noncrystalline one. To this end, we approximated the amorphous scattering by a 4th order polynomial and fitted it to the measured scattering curve at 5 points with minimum scattering. In this way we obtained the scattering relief of the noncrystalline portion only.

An example of background scattering reliefs is shown in Fig. 5. We note at once that the background is far from being homogeneous. Rather we observe clear

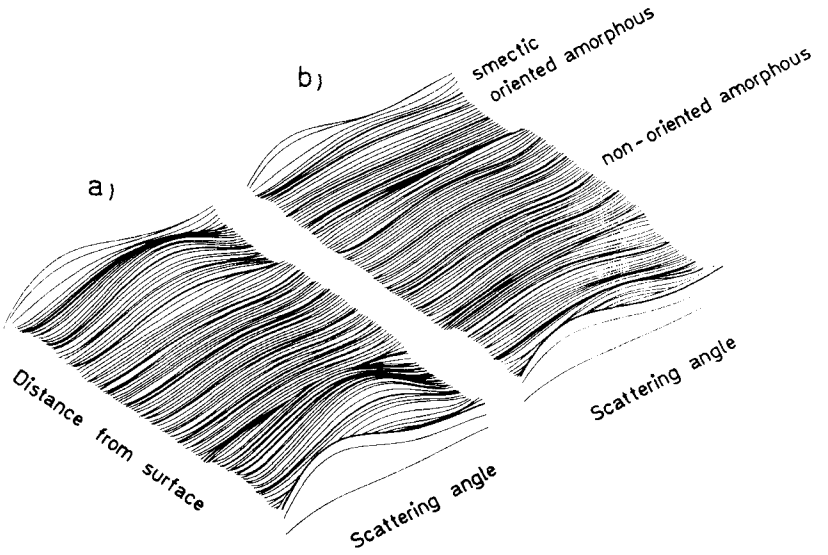

FIG. 5. These scattering reliefs show wide-angle x-ray scattering curves of the background scattering due to the amophous or smectic portion in the Daplen KS10 sample from Fig. 2 for two different directions of the x-ray beam: perpendicular to the flow direction (a) and parallel to the flow direction (b).

indications of orientation, particularly if we compare scattering reliefs which correspond to different directions of the x-ray beam. It is found that the orientation of the amorphous portion is highest near the surface and low in the core, thus imitating the behavior of the crystallites. Whenever we have a high crystalline orientation, we also find a high amorphous orientation. Only the rather homogeneous portion in the core, therefore, comes near to a truly "amorphous" and not oriented structure. But we observe one more thing: We clearly recognize a shift of the angular position of the maximum of background scattering toward smaller angles (from about 18° to about 15°) in the vicinity of the surface (that is, in the "skin layer").

We have arguments to ascribe the shift of the maximum background scattering as observed in Fig. 5 and in similar plots for several other samples to the occurrence of another form of PP which is mesomorphic, neither amorphous nor truly crystalline. In the literature (cf. Ref. 3), such a mesomorphic PP modification has been referred to as smectic or paracrystalline though its nature is still not completely understood; the mesomorphic modification has been observed with rapidly quenched PP. As can be seen from Fig. 3, the skin layer of the sample from Daplen KS10 exhibits weak reflections of α-PP. These certainly obscure the scattering of smectic PP. In scattering reliefs of samples from the less polydisperse Daplen PT55, on the other hand, reflections due to α-crystallites were found to be completely absent in the vicinity of the surface if the samples were taken far from the gate. In this case the measured scattering curves from the surface region showed only two broad maxima (at 15 and 21°); that is, the scattering behavior typical of the mesomorphic PP modification.

In Fig. 5, three discernible ranges of the noncrystalline portion are indicated: smectic, oriented amorphous, nonoriented amorphous. The symmetry of the structure is obvious.

The occurrence of the mesomorphic PP modification in the skin layer close to the surface is probably due to very fast cooling in this range. Its formation obviously depends on the processing parameters because this modification could not be observed with all samples investigated. We found that the smectic layer becomes thicker if higher end pressure is used (e.g., 300 vs 1500 bar).

Having found the astonishingly complex multilayered textures in our samples, we, of course, question their cause. Hydrodynamic forces will certainly play a role, the more so since, basically, several flow forms will be realized during the injection-molding process, as shown in Fig. 6. Near the confining walls in the mold, and also in the nozzle and the gate, shear flow will take place. This flow form has a rotational component, and therefore will lead to a dynamic orientation of 45° or less. However, whenever the flow is accelerated, for instance, by a funnel-shaped (converging) flow field, we will encounter elongational flow, which leads to a stable orientation parallel to the flow direction (0°). On the other hand, in fan-shaped (diverging) geometries we have compressional flow, the velocity is reduced, and we should eventually expect an orientation perpendicular to the flow direction (90°). Of course, this behavior is inferred from experience in model solutions and from theory. It also presumes a sufficiently anisotropic shape of the particles, which holds true for the molecules but not necessarily for the crystallites. And, of course, in reality hydrodynamics is only one of the acting forces, as cooling, orientation, nucleation, relaxation, and crystallization will take place simultaneously during the injection-molding process, and these altogether are responsible for the observed

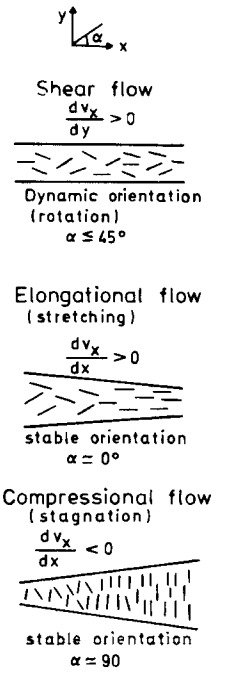

FIG. 6. Flow and orientation, shown schematically.

textures. In this context we refer to recent theoretical and experimental investigations of shear-induced crystallization of PP [9].

For the time being, the state of the experiments is as follows: We can, with good results, determine the rather complex local texture. We know possible causes for it (namely, the interplay of cooling, flow field, nucleation, relaxation, and crystallization). We have an abundance of structural data of the form shown in Figs. 2–5. However, the exact correlations between processing parameters and structure are still unclear, and our present understanding is in many parts only a qualitative one.

This work was begun in Project S3304 within the frame of a working party initiated by H. Janeschitz-Kriegl and sponsored by the FWF (Österreichischer Fonds zur Förderung der wissenschaftlichen Forschung). Most of the results presented here were obtained in FWF Project P7446, in close cooperation with other groups to whom we are grateful for the supply and the preparation of samples and for discussion. Intermediate reports have been published and are available [1, 2, 4, 5].

REGENERATED CELLULOSE FIBERS

For the past 50 years, viscose fiber has been the king of regenerated cellulose textiles. In its modern version, as, e.g., the modal or polynosic type, it has very good properties, and its fabrication process has the ripeness of old age. However, it has its shortcomings from the point of view of environmental problems. Therefore,

the search for new and more ecologically acceptable production processes is going on. On the one hand, new spinnable derivatives are sought; on the other hand, methods of dissolving cellulose directly in suitable solvents without a derivative detour are sought. So far, these new fibers have met with limited success.

We have studied the structure of one type of these new products in order to compare it with the well-known structure of cellulose fibers [10]. A comparison is made in Fig. 7 between various fiber types, namely regular viscose fibers, modal fibers, and polynosics on the one hand, and the new solvent-spun fibers NMMO (cellulose in *N*-methylmorpholine-*N*-oxide) and DMAc/LiCl (cellulose in dimethylacetamide + LiCl). The latter two types are called "lyocell fibers" by their generic name. Additionally, we have included a fiber named "carbamate," which is spun from a solution of cellulose carbamate in sodium hydroxide, and decomposed after spinning. In Fig. 7 the tensile strength is plotted against the crystalline orientation factor f_{cr} as determined in the usual way by means of WAXS (wide angle x-ray scattering). We note that the steeper line comprises the "good" fibers (viscose, modal, polynosic, NMMO); here an increase in f_{cr} brings about a higher gain in tensile strength. A lower line is found for the poor fibers (DMAc/LiCl, carbamate). As only the NMMO fibers compares satisfactorily with the viscosics, we have studied only this product. In the following it is called a lyocell fiber.

Results concerning general structural and textile properties have been published [11]. The lyocell fiber NMMO has good textile properties. One important disadvantage is its high fibrillability, mainly in the swollen state, which is not found with viscose-type fibers. We tried to elucidate the structural differences giving rise to this behavior. To this end, we have undertaken WAXS studies of fibers after swelling in NaOH. We determined the following figures.

Long periods: The long periods L give us the combined length of both crystallites and amorphous regions. It is well known that distinctive meridian long-period interferences with regenerated cellulose fibers are found only after hydrolysis. However, after treatment with NaOH we found distinctive shoulders which could be evaluated to give a figure for the length of the long period.

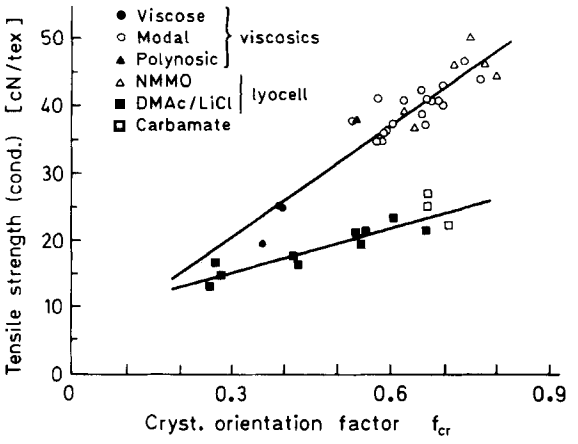

FIG. 7. Tensile strength as a function of the orientation factor f_{cr} for different fibers.

Crystallite length: The crystallite length was determined from the linewidth of the meridian reflexes in the WAXS diagram. To this end, the linewidth was determined for the reflexes (020) and (040), extrapolated to zero angle, and from this value the crystallite length was calculated in the usual way (Scherrer formula). The crystallite length, L_{cr}, is, of course, smaller than the long period L because it refers to the crystallite itself.

Crystallinity: This figures was determined by means of WAXS in the usual way.

Orientation factor: The crystalline orientation factor f_{cr} was determined by means of WAXS. In addition, an amorphous orientation factor f_{am} was determined by means of WAXS and birefringence measurements, as described elsewhere [12].

From our measurements, some general features can be read immediately. For lyocell, the intensity of the long period L is lower than for viscose fibers. This means that in this fiber we have a lower difference between crystalline and amorphous regions in both order and orientation. In water (and NaOH) the crystallinity goes down, but not so the orientation! Therefore, we presume that in the highly swollen state we find a nematic or smectic structure rather than complete disordering. A closer inspection shows clear differences in crystallinity and orientation between both fiber types, as shown in Fig. 8, which compares lyocell (NMMO) and modal. We find a much higher crystallinity in lyocell; especially so in the fiber direction (as obtained from a comparison between long period L and crystallite length L_{cr}). The ratio between crystalline and amorphous orientation is much smaller for lyocell, indicating rather homogeneously structured elementary fibrils. Finally, we have listed the mass fractal dimension D_m, which we had determined in an earlier paper from the SAXS curve (small-angle x-ray scattering) [13].

What can we derive from these data? We propose the structure shown schematically in Fig. 9. Thus, in the lyocell fibers we have rather long crystallites (91%) which are joined by only small amorphous regions. With modal fibers, the crystallite length is only 66% of the total. Obviously, the elementary fibrils in lyocell are compacted structures. In addition, the lyocell fibers show, due to their low amorphous portion, hardly any crosslinks between different elementary fibrils, and therefore little clustering as is found with viscose-type fibers. These two facts can easily explain the higher fibrillability: since the lyocell fibers have rather isolated, compact elementary fibrils, these can be easily separated by mechanical treatment, thereby

	Crystallinity		Crystallinity in fiber direction		Orientation factor ratio	Long period / Crystallite length	Mass fractal Dimension D_m
		ratio		ratio	f_{cr} / f_{am}		
Lyocell	0.61	1.6	0.9	1.6	1.4 - 1.7	1.15	1.67
Modal	0.38		0.55		5 - 10	1.8	1.27

FIG. 8. Tabulated comparison of structure parameters for both lyocell and modal fibers.

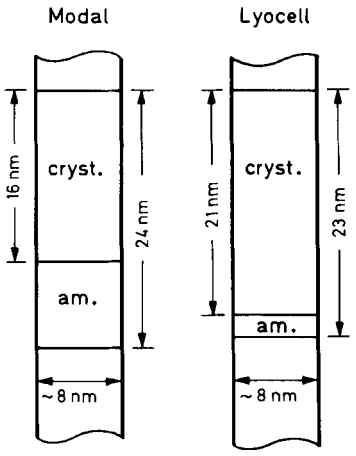

FIG. 9. Structure model for the elementary fibril of both modal and lyocell fibers.

leading to fibrillation. The modal fibers have shorter, partly clustered crystallites which lead to lateral strength and prevent fibrillation. The cluster formation may also be responsible for the lower fractal dimension D_m, as shown in Fig. 8. Although the ratio between f_{cr} and f_{am} is high in the modal fibers, a noticeable amorphous orientation is present. This underlines the importance of the amorphous orientation for the textile properties. We suggest that for a certain fiber type, the amorphous orientation will determine its elongation: the latter will be high if f_{am} is low. We conclude that the amorphous regions, their orientation and structure, probably play a much more important role for the properties of cellulose fibers than was assumed in the past. For synthetic fibers, this connection is known.

What is the reason for these differences in fiber structure? Probably it is the spinning method. In the old viscose processes, the dissolved macromolecules exist as completely disordered, coiled chain molecules. During fiber formation, they not only must be oriented to form the crystallites, but in addition a decomposition must take place, since we are dealing with a cellulose derivative. With the new solvents, cellulose as such is dissolved. Therefore, no decomposition is required. In addition, the solution is probably not completely disordered, so that the dissolved macromolecules are already somewhat oriented before fiber formation due to the large draw-down ratio between spinneret and coagulation bath. It is known from the literature [14] that concentrated solutions of the type used in lyocell processes tend to form liquid crystals (above 20%), although the spinning solutions have not been found to do so in this state. Therefore, in these new solvent-spinning methods, orientation and structure formation during the spinning process will be much easier. The different possibilities of fiber spinning are shown schematically in Fig. 10. Melts consist of coiled and entangled chain molecules. If spun without stretching, they will form folding crystals. Derivative solutions of the old type, such as viscose, consist of coiled chain molecules too. Therefore, the spinning process is rather complicated, and to obtain good fibers a delicate stretching process must be added after precipitation and decomposition of the derivatives. For liquid crystal solutions, matters are much easier, and both crystallite formation and orientation are greatly facilitated.

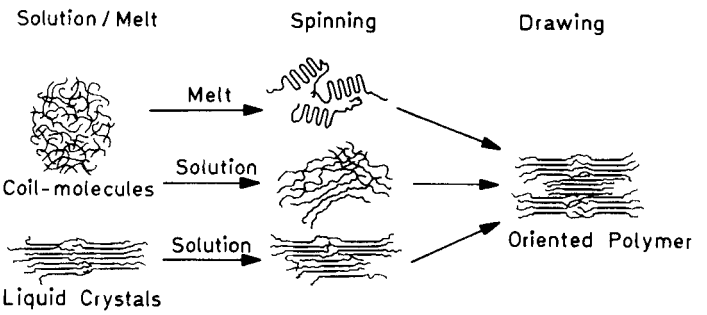

FIG. 10. Orientation and fiber formation during spinning shown schematically.

It appears that we are not yet able to control this new process properly, but its intrinsic advantages will certainly come to bear in the future.

The difference between melts and solution lies in the fact that in melts the macromolecules have only partners of the same kind. Therefore, in spite of entanglements, they are in an ideal, rather flexible state, and have undisturbed coil dimensions. On the other hand, solutions are not ideal. They have different neighbors, namely the solvent molecules, and are therefore mostly stiffened due to solvation. Their dimensions are changed; generally we find an extension of the coil. Only the θ-state approximates the undisturbed chain; it represents a pseudoideal solution state which critically depends on solvent composition, temperature, and pressure. Thus, as a rule we will find solvated and therefore more extended and stiffer macromolecules in solution as compared with melts.

Of course, these considerations call for a thorough and systematic rheological study of both the new types of solutions and of the spinning process. It is hoped that this badly needed information will be available soon.

ENZYMATIC DEGRADATION OF CELLULOSE

Cellulose can be degraded to fermentable glucose by means of the enzyme complex cellulase, which consists essentially of exoglucanase, endoglucanase, and β-glucosidase. It is assumed that during this process, endocellulase serves to start the degradation, while the exocellulose finishes the job down to cellobiose, which is then degraded to glucose by β-glucosidase. In our studies on the parameters controlling this degradation reaction, we have found that it represents an "all or nothing" process [15]. That means a cellulose chain is either completely degraded or not at all. We have found that during heterogeneous degradation, the important structural parameters do not change. The parameters studied were crystallinity (x-ray), intrinsic viscosity (in EWNN), and inner specific surface (SAXS). As we note from Fig. 11, all these parameters change but little or not at all during degradation for a reaction time of 48 hours. It was these finding which prompted us to propose our "all or nothing" model. However, in the course of our degradation experiments with native cellulose, especially with wood pulp, we found a peculiar trait in the kinetics: It turned out to be a two-step process consisting of two straight lines in the

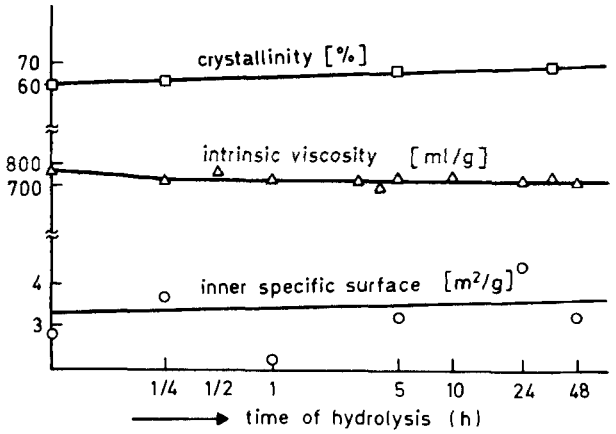

FIG. 11. Variation of the parameters crystallinity, inner specific surface, and intrinsic viscosity during enzymatic degradation of a bleached spruce sulfite pulp.

usual first-order kinetics plot of log residual cellulose vs time. In Fig. 12 this is shown for a wood pulp (spruce sulfite, bleached) for two concentrations of the pulp dispersion. We readily observe a biphasic first-order reaction. The transition point is not related to any one of the structural parameters. It looks as if the pulp consisted of two phases with different accessibility [17]. However, to our great surprise this behavior was not found with regenerated cellulose (viscose fibers) [18],

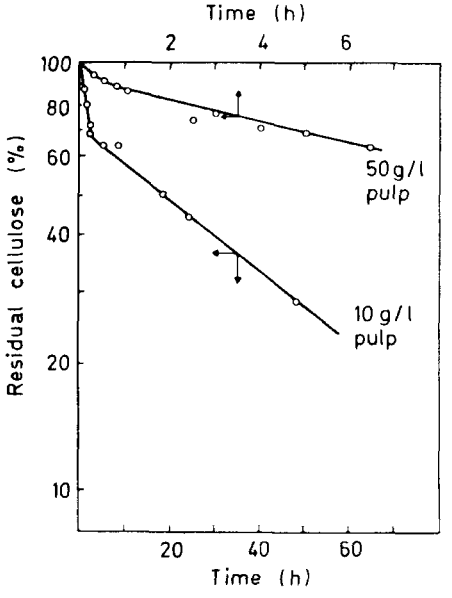

FIG. 12. Kinetics of enzymatic degradation of a bleached spruce sulfite pulp with variation of the pulp concentration (biphasic first-order reaction).

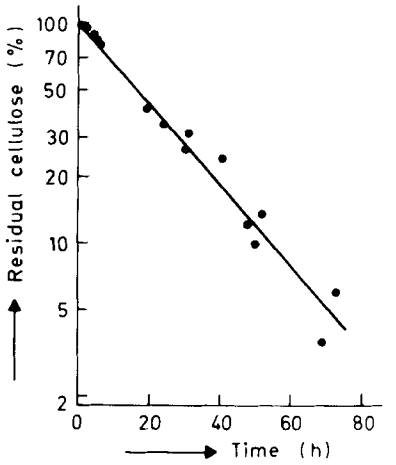

FIG. 13. Kinetics of the enzymatic degradation of a regenerated cellulose fiber (viscose) (monophasic first-order reaction).

as shown in Fig. 13. Since obviously the main parameters for accessibility, namely crystallinity and inner surface, are not responsible for this peculiar behavior, we had to ask the question: Why does cellulose behave in this way?

Our experiments showed that in the case of wood pulp, the fast reaction comprised about 30–50% of degraded material. Its amount could be varied by pretreatment: Suitable treatment increased both the slope of the reaction line and the percentage of the fast reaction. The slow reaction led, within a reasonable time, to only 50–70% conversion of total cellulose. To enhance the conversion, very long times had to be used. The influence of the enzyme concentration, c_E, was variable. It accelerated the reaction only up to a certain limit, which was about 40 mg/g for the fast reaction and about 10 mg/g for the slow reaction. Beyond these values, no influence was found. In order to find an explanation for this behavior, we had to take into account the structure of the enzyme molecule. Studies at our institute had led to the so-called "tadpole model" (Fig. 14) for exocellulase, consisting of a head,

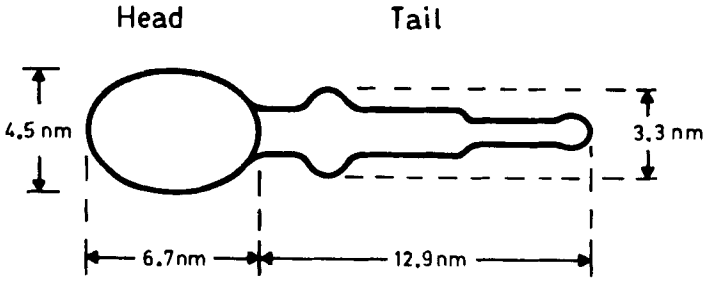

FIG. 14. Model of the enzyme exocellulase as determined by SAXS scattering.

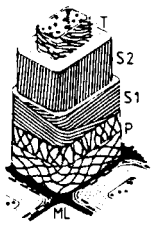

Middle lamella				Lignin and hemicelluloses
Primary wall	P	5-10%	increasing order	Fibrils disordered
Secondary wall	S_1	12-16%		Loose spiral fibrils
	S_2	70-90%		Tight, crossing fibrils
	S_3			
Tertiary wall	T	4-8%		Disordered fibrils, polyoses

FIG. 15. The wood cell wall, shown schematically.

which degrades, and a tail, which is responsible for the adsorption of cellulase at the substrate [19]. Obviously, the tail needs voids in the cellulose fibrils in order to adsorb. We have reasoned that the two-phase degradation is caused by a two-phase adsorption. But what causes the two-phase adsorption, and why are native and regenerated celluloses different? The answer may lie in the texture of native celluloses. The architecture of a wood cell, as shown in Fig. 15, shows a very intricate texture [20]. It consists of a layered buildup. The middle lamella represents a hydrophobic coating, which protects against attack by solvents and microorganisms. Following this, we find a primary wall with disordered fibrils, followed by the secondary walls S_1, S_2, and S_3. These consist of spiraled fibrils, which in S_2 (the main portion) are very tight. Now, in order to make pulp out of wood, both the middle lamella and the primary wall must be more or less digested, and even the S_1-layer may be attacked. Pretreatment of the pulp will enhance this action, so that eventually we have a rather loose outer layer, extending to P and perhaps S_1, and a tight inner layer. These two layers will, of course, show greatly differing accessibilities, and therefore greatly different adsorptions of cellulase. In this way, a two-phase adsorption will take place. In this model, the extent of the accessible and loose outer layer with high adsorption will, of course, depend on the intensity of both pulping and pretreatment, and must therefore be variable. However, it will not depend on structural parameters, as does crystallinity, or the inner surface. Thus, we assume that the loosened outer layer is responsible for high adsorption and fast reaction, while the intact inner layer shows poor adsorption and slow reaction.

If we accept two-phase adsorption for the native celluloses, we can formulate it with the help of the Langmuir adsorption isotherm. Our two-step kinetics follows an equation of the type

$$-(dc/dt) = k_1c_1 + k_2c_2$$

with cellulose concentration $c = c_1 + c_2 = c(a_1 + a_2)$, where a_1 and a_2 are the accessibilities for the fast and the slow reactions, respectively. In our reasoning, the accessibilities a are defined in terms of adsorptivity. So a_1 is a measure for the fraction of adsorption sites characterized by the adsorption coefficient K_1. Their coverage (fraction of the surface covered) is given by the coverage parameter (θ_1). a_2 is defined in the same way by K_2. The kinetics will, in general, depend on two velocity constants k_1 and k_2, on the structurally determined accessibility parameters a_1 and a_2, and on the respective coverage parameters θ_1 and θ_2, which are controlled by the respective adsorption constants K_1 and K_2.

We obtain

$$-(dc/dt) = k_1 a_1 \theta_1 c_1 + k_2 a_2 \theta_2 c_2$$

with

$$\theta_i = \frac{K_i c_E}{1 + K_i c_E}, \qquad c_E = \text{enzyme concentration}$$

Because θ depends in a somewhat complex way on both the adsorption constant K and the enzyme concentration c_E, we expect a corresponding behavior. However, some simplifications are possible. First, we assume that the differences in the kinetics are brought about only by structural features and adsorptivity. Therefore, we put $k_1 = k_2 = k$. Now we have

$$-(dc/dt) = kc(a_1\theta_1 + a_2\theta_2)$$

Furthermore, we will regard the limiting cases. In the beginning of adsorption, we have a linear range. This linear range can be approximated by $\theta_1 = K_i c_E$ for both θ_1 and θ_2. In this case two-step kinetics is to be expected, controlled by K_1 and K_2, but also dependent on the enzyme concentration c_E. The final stage of absorption can be approximated by the assumption of saturation. If both adsorption regions are saturated, we find $\theta_1 = \theta_2 = 1$, and two-phase kinetics is caused only by the structural parameters a_1 and a_2. However, it should no longer depend on the enzyme concentration c_E.

As our experiments show, we actually observe a transition from enzyme-dependent kinetics to an independent one, in agreement with the two limiting cases of the adsorption isotherm. The overall saturation concentration c_E has been given in the literature as 92 mg/g or less for Avicell microcrystalline cellulose [21].

With regenerated cellulose, on the other hand, we find no texture or layer system. Rather, the viscose fibers consist of a uniform network of crosslinked and possibly clustered fibrils, whose accessibility is rather homogenous. Therefore, we will also have uniform adsorption throughout the fibers, and therefore one-phase kinetics, as observed experimentally.

However, some additional findings must be reported which show the sensitivity of the enzymic reaction to structural traits [22]. With regular viscose fibers, the one-step reaction is retained even after partial HCl-hydrolysis. It is different with modal fibers: Here the treatment leads to a two-step reaction, and the velocity of the fast reaction corresponds to that of the one-step reaction in regular viscosics. We assume that in modal fibers, HCl treatment leads to chain splitting and recrystallization (and the appearance of pronounced long-period interferences), and in consequence brings about a reordering with the provision of new sites of easy attack for the enzyme. Interestingly enough, native fiber cotton also shows a one-step enzymatic degradation [23]. This is probably due to the absence of any aggressive pretreatment, contrary to the pulp fibers.

We may infer from these results that in the one-step degradation of the cellulosic fibers cotton, viscose, and untreated modal, the enzyme will attack the fibers only at their homogenous surface. The production of a more easily degradable component by partial hydrolysis with HCl in modal fibers can be explained by the

appearance of new crystallite surfaces and edges, which are obviously favorable for enzymatic attack.

REFERENCES

[1] P. Zipper, A. Jánosi, E. Wrentschur, and P. M. Abuja, *J. Appl. Crystallogr., 24*, 702–708 (1991).

[2] P Zipper, A. Jánosi, E. Wrentschur, C. Knabl, and P. M. Abuja, *Österr. Kunstst.-Z.*, Submitted.

[3] S. Brückner, S. V. Meille, V. Petraccone, and B. Pirozzi, *Prog. Polym. Sci., 16*, 361–404 (1991).

[4] E. Fleischmann, P. Zipper, A. Jánosi, W. Geymayer, J. Koppelmann, and J. Schurz, *Polym. Eng. Sci., 29*, 835–843 (1989).

[5] P. Zipper, A. Jánosi, and E. Wrentschur, *Österr. Kunstst.-Z., 21*, 54–59 (1990).

[6] F. L. Binsbergen and B. G. M. De Lange, *Polymer, 9*, 23–40 (1968).

[7] J. P. Trotignon and J. Verdu, *J. Appl. Polym. Sci., 34*, 1–18 (1987).

[8] A. Turner-Jones, J. M. Aizlewood, and D. R. Beckett, *Makromol. Chem., 75*, 134–158 (1964).

[9] G. Eder, H. Janeschitz-Kriegl, and S. Liedauer, *Prog. Polym. Sci., 15*, 629–714 (1990).

[10] J. Lenz and J. Schurz, *Cellul. Chem. Technol., 24*, 3–21, 679–692 (1990).

[11] J. Lenz, J. Schurz, and E. Wrentschur, *Papier, 42*, 683–689 (1988); *J. Appl. Polym. Sci., 35*, 1987–2000 (1988); *Holzforschung, 42*, 117–122 (1988).

[12] J. Lenz, J. Schurz, and E. Wrentschur, *Acta Polym., 43*, 307–372 (1992).

[13] J. Lenz and J. Schurz, *Holzforschung, 44*, 27–228 (1990).

[14] P. Weigel, R. Hirte, D. Zeuke, and J. Hartmann, *Acta Polym., 335*, 83–88 (1984). H. Finkelmann, *Angew. Chem., 99*, 840–848 (1987). M. Siekmeyer, H. Steinmeier, and P. Zugenmaier, *Angew. Makromol. Chem., 166/167*, 131–138 (1989).

[15] J. Schurz, *Holzforschung, 40*, 225–232 (1986). W.-D. Eigner, A. Huber, and J. Schurz, *Cellul. Chem. Technol., 19*, 579–589 (1985).

[16] J. Schurz, J. Billiani, A. Hönel, W. D. Eigner, A. Jánosi, M. Hayn, and H. Esterbauer, *Acta Polym. 36*, 76–80 (1985).

[17] H. Esterbauer and A. Jánosi, *Papier, 38*, 599–606 (1984).

[18] J. Schurz and A. Hönel, *Cellul. Chem. Technol., 23*, 465–476 (1989).

[19] P. M. Abuja, I. Pilz, M. Caeyssens, and P. Tomme, *Biochem. Biophys. Res. Commun., 156*, 180–185 (1988).

[20] D. Fengel and G. Wegener, *Wood Chemistry, Ultrastructure, Reactions*, Walter de Gruyter, Berlin, 1984.

[21] W. Sattler, H. Esterbauer, O. Glatter, and W. Steiner, *Biotechnol. Bioeng., 33*, 1221–1234 (1989).

[22] J. Lenz, J. Schurz, and H. Esterbauer, *Papier, 44*, 656–661 (1990). J. Lenz, H. Esterbauer, W. Sattler, J. Schurz, and E. Wrentschur, *J. Appl. Polym. Sci., 41*, 1315–1326 (1990). H.-P. Fink, B. Philipp, C. Zschunke, and M. Hayn, *Acta Polym., 43*, 270–274 (1992).

[23] K. Selby, *Adv. Chem. Ser., 95*, 149 (1968).